ADVANCED FUNCTIONAL MATERIALS
www.afm-journal.de

Copper@ZIF-8 Core-Shell Nanowires for Reusable Antimicrobial Face Masks

Abhishek Kumar, Anu Sharma, Yi Chen, Megan M. Jones, Stephen T. Vanyo, Changning Li, Michelle B. Visser, Supriya D. Mahajan, Rakesh Kumar Sharma, and Mark T. Swihart**

SARS-CoV-2 and other respiratory viruses spread via aerosols generated by infected people. Face masks can limit transmission. However, widespread use of disposable masks consumes tremendous resources and generates waste. Here, a novel material for treating blown polypropylene filtration media used in medical-grade masks to impart antimicrobial activity is reported. To produce thin copper@ZIF-8 core-shell nanowires (Cu@ZIF-8 NWs), Cu NWs are stabilized using a pluronic F-127 block copolymer, followed by growth of ZIF-8 to obtain uniform core-shell structures. The Cu@ZIF-8 NWs are applied to filtration media by dip coating. Aerosol filtration efficiency decreases upon exposure to ethanol (solvent for dip-coating), but increases with addition of Cu@ZIF-8 NWs. Cu@ZIF-8 NWs shows enhanced antibacterial activity, compared to Cu NWs or ZIF-8 alone, against *Streptococcus mutans* and *Escherichia coli*. Antiviral activity against SARS-CoV-2 is assayed using virus-infected Vero E6 cells, demonstrating 55% inhibition of virus replication after 48 h by 1 µg of Cu@ZIF-8 NWs per well. Cu@ZIF-8 NWs' cytotoxicity is tested against four cell lines, and their effect on inflammatory response in A549 cells is examined, demonstrating good biocompatibility. This low-cost, scalable synthesis and straightforward deposition of Cu@ZIF-8 NWs onto filter media has great potential to reduce disease transmission, resource consumption, and environmental impact of waste.

1. Introduction

The ongoing pandemic caused by the SARS-CoV-2 virus has brought the world to a halt. The virus has proven highly contagious, with more than 53 million cases reported worldwide (at the time of writing).[1] Although there are uncertainties associated with precise modes of transmission of the coronavirus disease 2019 (COVID-19), current evidence leads most experts to believe that like other respiratory virus infections, it spreads through direct and indirect human contact, respiratory droplets (diameter ≥5 µm), and fine-particle aerosols (diameter ≤5 µm).[2,3] The use of face masks can help in controlling the spread of these viruses by capturing droplets and aerosol particles generated when an infected person speaks, exhales, coughs, or sneezes.[4] While N95 masks are effective in capturing these particles, with an efficiency of 95%, their limited reusability has led to shortages for medical workers and limited availability for others.[5] While the shortage of N95 masks continues, cloth masks or homemade masks are recommended for use by the general public.[6] Some combinations of materials such as cotton-silk or cotton-chiffon have shown >80% efficiency in capturing fine aerosol particles (diameter <300 nm) and >90% efficiency in capturing larger particles.[7] Disposable surgical masks are also effective in capturing these respiratory droplets with some limitations.[8] Most medical-grade facemasks are disposable or reusable for a limited time. With hundreds of millions of such masks produced daily, their production and disposal consume substantial resources. Reusable antibacterial face masks have been in development for years;

A. Kumar, A. Sharma, Y. Chen, Prof. M. T. Swihart
Department of Chemical and Biological Engineering
University at Buffalo (SUNY)
Buffalo, New York 14260, USA
E-mail: swihart@buffalo.edu

A. Sharma, Dr. R. K. Sharma
Department of Chemistry
University of Delhi
Delhi 110007, India
E-mail: sharmark@chemistry.du.ac.in

Dr. M. M. Jones, S. T. Vanyo, Prof. M. B. Visser
Department of Oral Biology
University at Buffalo (SUNY)
Buffalo, New York 14214, USA

The ORCID identification number(s) for the author(s) of this article can be found under https://doi.org/10.1002/adfm.202008054.

Dr. C. Li
Department of Biomedical Engineering
University at Buffalo (SUNY)
Buffalo, New York 14260, USA

Prof. S. D. Mahajan
Department of Medicine
Division of Allergy, Immunology and Rheumatology
Jacobs School of Medicine and Biomedical Sciences
University at Buffalo (SUNY)
Buffalo, New York 14260, USA

Prof. M. T. Swihart
RENEW Institute
University at Buffalo (SUNY)
Buffalo, New York 14260, USA

DOI: 10.1002/adfm.202008054

however, they are needed now more than ever to help reduce shortages of masks as well as reduce the waste generated through use of disposable face masks.[9,10]

Various materials have been tested for making antibacterial face masks including silver,[9,11] copper and oxides of copper,[12,13] titanium dioxide,[14] and graphene.[15,16] Inorganic nanomaterials of noble metals have garnered much interest for their antibacterial activity.[17] Copper is much less expensive than other noble metals, and has been used for centuries for its biocidal properties.[18] Copper nanoparticles show excellent antibacterial ability for both gram-positive and gram-negative bacteria.[19] Moreover, copper and brass (an alloy of copper and zinc) have been proven to be effective against human coronoavirus 229E; viruses are destroyed rapidly on brass within a few minutes following simulated fingertip contamination.[20] A more recent study confirms that finding and reports rapid decay in SARS-CoV-1 and SARS-CoV-2 viruses within 4 and 8 h of exposure on copper surfaces while they remained viable for up to 72 h on plastic and stainless steel surfaces.[21] Copper nanoparticles release copper ions that are responsible for the generation of reactive oxygen species (ROS), which damage DNA and cause bacterial protein and lipid peroxidation.[22–27] The shape of nanomaterials can also play an essential role in their antimicrobial activity. For example, triangular silver nanoplates showed higher biocidal activity compared to spherical nanostructures against strains of *Escherichia coli* (*E. coli*). This improved performance was attributed to more active {111} planes.[28] Metallic nanowires have some inherent advantages over other nanostructures such as high surface-to-volume ratio, and surfaces bounded by highly active facets.[29] However, excessive ROS generation leads to cytotoxicity, and this could be a major hurdle for the use of copper nanomaterials in applications where they contact human tissues. The risk of copper-induced toxicity can be reduced by slowing the release of copper ions.[25,31,32] Coating with materials such as metal-organic frameworks (MOFs) and polymers could be the best approach to reducing its toxicity while maintaining antimicrobial activity.

MOFs have highly ordered and porous crystalline structures that provide a variety of chemical and physical properties that make them suitable for adsorption of hazardous substances, catalysis, drug delivery, and antimicrobial applications.[33,34] Zeolitic imidazolate framework 8 (ZIF-8) is a porous MOF that is easy to synthesize under ambient conditions and has promising applications in catalysis, imaging, gas storage, and antibacterial applications.[35,36] Nanowire@MOF core-shell heterostructures are a growing research area. In many cases, this combination of components provides enhanced performance compared with a single material.[37–40] These core–shell heterostructures can exhibit synergistic properties that open up new applications. Such structures have been prepared by using MOFs as a template or by loading nanoparticles within cavities in MOFs. Core-shell heterostructures are particularly promising structures for the adsorption and degradation of micropollutants present in water, because the ZIF-8 shell can drive adsorption, while the reactive core can slowly release copper ions that provide antibacterial activity and promote pollutant degradation. In contrast to the hydrophilic Ag NW cores in structures such as Ag@ZIF-8 NWs,[39,41] Cu NWs are synthesized using hydrophobic surfactants and often require further processing such as coating with a hydrophilic polymer like polyvinylpyrrolidone (PVP) to make them stable in polar solvents used for ZIF-8 growth.[40] Moreover, PVP prevents degradation of Cu NWs from hydronium ions released during the formation of ZIF-8.[42] However, our initial results working with thin Cu NWs indicated that PVP was not effective for producing a stable suspension of these NWs in polar solvents required for stability and uniform coating of ZIF-8.

Pluronic F-127 is a triblock copolymer with excellent biocompatibility and low toxicity. Its amphiphilic structure makes it an ideal candidate for oil-to-water phase transfer of hydrophobic drugs and nanoparticles, facilitating their use in drug delivery, bioimaging, and other biomedical applications.[43] Here, we report for the first time a low-cost and efficient method for the synthesis of thin Cu@ZIF-8 NWs using a pluronic block copolymer as a stabilizing and surface passivating agent. Cu@ZIF-8 NWs show enhanced thermal stability and sustained release of Cu ions. We observed significant antibacterial activity against gram-positive and gram-negative bacterial species, *E. coli* and *Streptococcus mutans* (*S. mutans*), confirming Cu@ZIF-8 NWs, potential as an antibacterial agent. Additionally, we demonstrate that the prepared nanocomposite can be easily attached to the fibers of facemasks paving the way for reusable antimicrobial facemasks and other textiles.

2. Results and Discussion

2.1. Synthesis and Characterization of Cu@ZIF-8 NWs

Figure 1 schematically illustrates the simple and scalable synthesis route for producing Cu@ZIF-8 NWs. The Cu NWs were prepared using a modified one-pot synthesis route with OAm as a surface capping agent.[30] Cu NWs are unstable and are quickly oxidized during ZIF-8 synthesis in polar solvents due to hydronium ions released during ZIF-8 formation. Surface passivation is required in such cases to prevent Cu NW degradation. Therefore, we first coated Cu NWs with pluronic to stabilize them. A layer of ZIF-8 was then grown on the surface of Cu NWs to produce a core-shell structure by first adding $Zn(OAc)_2.2H_2O$ salt, then 2-methylimidazole.

Figure 2 illustrates the morphology and structure of the synthesized nanomaterials. Figure 2a–d shows transmission electron microscopy (TEM) images of the Cu NWs, with diameters of 20–35 nm. Figure 2i shows a scanning electron microscopy (SEM) image of the Cu NWs. The length of Cu NWs ranged from 5 to 10 µm. Both the diameter and length of Cu NWs were related to the amount of OAm used in the synthesis. On decreasing the amount of OAm from 5 to 2.5 mL per batch, the diameter more than doubled and the length exceeded 20 µm (Figure S1a,b, Supporting Information). Although Cu NWs of larger length are desired for many applications,[37] we observed that the Cu NWs synthesized using this lower amount of OAm were often entangled, which complicates their separation and handling. Moreover, for Cu@ZIF-8 NW core-shell structures, we decided to use Cu NWs of smaller diameter because thinner nanowires will provide a higher ZIF-8 fraction, higher Cu@ZIF-8 interfacial area, and shorter transport distance across

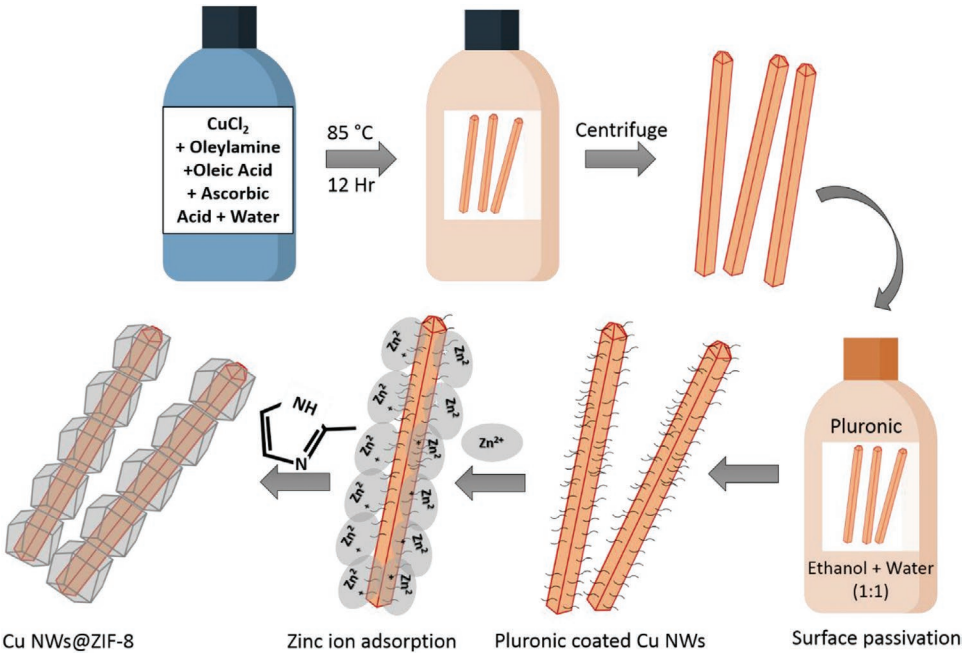

Figure 1. Schematic representation of the synthesis of core-shell Cu@ZIF-8 NWs.

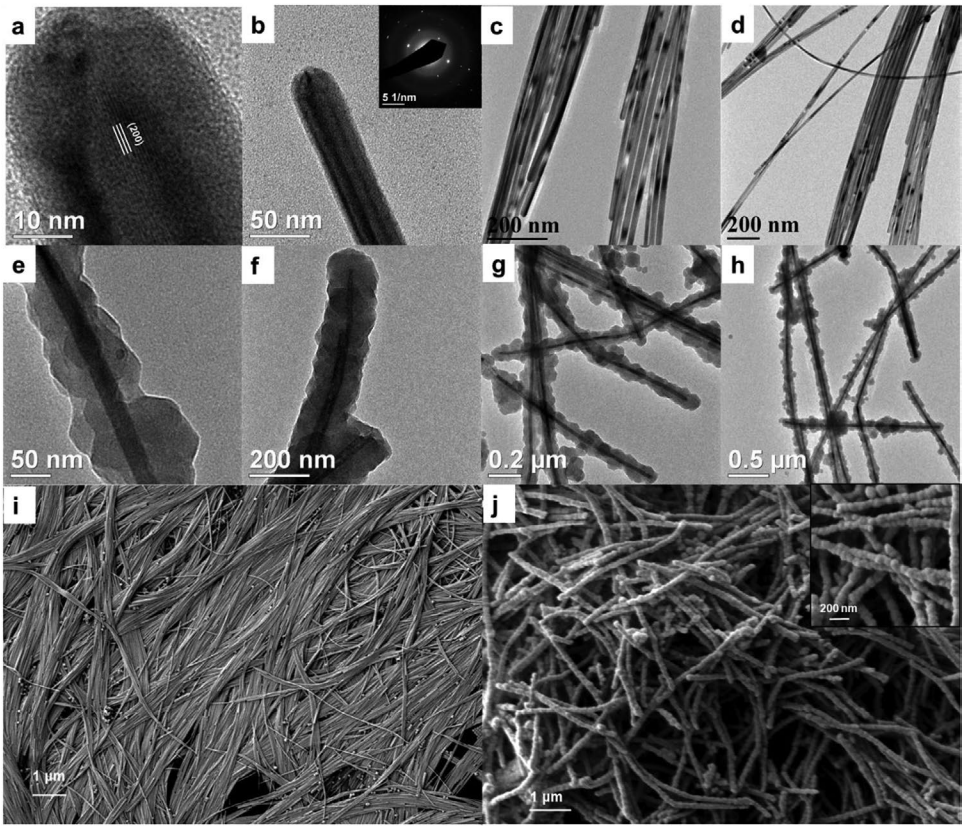

Figure 2. TEM images of a–d) Cu NWs, e–h) Cu@ZIF-8 NWs. The inset in (b) shows a representative SAED pattern from a Cu NW. SEM images of i) Cu NWs, j) Cu@ZIF-8 NWs.

the ZIF-8. These are desirable features for our application, but may not be optimal in other cases. Figure 2e–h presents TEM images of Cu@ZIF-8 NWs that are 60–100 nm in diameter. A uniform layer of ZIF-8 is visible on the surface of the Cu NWs. Figure 2j presents an SEM image of Cu@ZIF-8 NWs. A bead-like 1D structure can be seen in the SEM image, confirming uniform coating of Cu NWs with ZIF-8 and showing that they maintain their length of several microns.

The crystal structures of the nanomaterials were studied by X-ray Diffraction (XRD). Figure S3, Supporting Information, presents XRD patterns of the Cu NWs, ZIF-8 alone, and Cu@ZIF-8 NWs. For Cu NWs, three peaks are observed at $2\theta = 43.2$, 50.3, and 74.1° corresponding to the (111), (200), and (220) planes of face-centered cubic Cu, respectively (JCPDS card no. 04–836). Furthermore, absence of peaks for the oxides of copper such as Cu_2O or CuO indicates that the nanowires were not oxidized. The XRD pattern of Cu@ZIF-8 NWs displayed peaks corresponding to both Cu and ZIF-8.

Pluronic played a critical role in synthesis of Cu@ZIF-8 NWs. ZIF-8 formation is accompanied by release of hydronium ion into the solvent that decreases the pH of the solution. Bare Cu NWs then dissolve into the solution, disintegrating and leaving hollow ZIF-8 tubes. In our synthesis of Cu@ZIF-8 NWs, we often encountered this situation in which Cu NWs would dissolve leaving 1D hollow ZIF-8 nanostructures (Figure S3a,b, Supporting Information). Prior studies used PVP as a surface passivating agent to form Cu@ZIF-8 NWs.[40,42] However, coating thin Cu NWs with PVP poses certain problems such as Cu NW disintegration (PVP is a mild reducing agent), and incomplete passivation of the Cu NW surface. Due to these problems, the thin Cu NWs produced here were not effectively stabilized by PVP and often dissolved during ZIF-8 growth (Figure S3c,d, Supporting Information). These complications were overcome by using pluronic as the surface passivating agent.

Thermal stability (Figure S4a, Supporting Information) of the Cu@ZIF-8 NWs was studied using thermogravimetric analysis (TGA) under N_2 from 25 to 800 °C at a ramp rate of 5 °C min^{-1}. Between 25 and 100 °C, the initial weight loss of ≈3% is due to moisture adsorbed on the surface of the sample. Weight loss of ≈12% is observed between 100 and 400 °C corresponding to loss of OAm and pluronic. Finally, a sharp dip of about 60% in the TGA curve between 400 and 800 °C is attributed to the decomposition of the organic components of ZIF-8. N_2 adsorption (Figure S4b, Supporting Information) studies were carried out for Cu@ZIF-8 NWs and ZIF-8 synthesized following the same procedure. The Brunauer–Emmett–Teller (BET) surface area and pore volume of the sample decreased from 893 m^2 g^{-1} and 0.613 cm^3 g^{-1} for pure ZIF-8 to 583 m^2 g^{-1} and 0.399 cm^3 g^{-1} for Cu@ZIF-8 NWs. This decrease in surface area and pore volume is due to the nonporous Cu NW core that adds mass but does not add surface area or pore volume. Results of the BET study are summarized in Table S1, Supporting Information. The ratio of copper to zinc in the Cu@ZIF-8 NWs was determined by energy-dispersive X-ray spectroscopy. Figure S5, Supporting Information, presents a representative EDS spectrum from Cu@ZIF-8 NWs. A mean Cu:Zn ratio of 2.09:1 with a standard deviation of 0.17 was obtained based on three readings from different locations on the same sample. Assuming that the formula weight of ZIF-8 is 227.58 g mol^{-1}, with 28.7 wt% zinc which means, for every gram of copper nanowire, we have 1.667 g of ZIF-8. This is consistent with the larger volume of ZIF-8 compared with Cu (also due to its lower density) observed in TEM imaging.

The Fourier Transform Infrared spectra (FT-IR) of ZIF-8, Cu NWs coated with pluronic and Cu@ZIF-8 NWs are presented in Figure S6, Supporting Information. In the FTIR spectrum of ZIF-8, the peaks at 1312 and 1144 cm^{-1} are due to C—N stretching. The peaks at 757 and 686 cm^{-1} correspond to Zn—O and Zn—N stretching modes. The presence of these groups confirms the existence of the imidazole ring.[44] The spectrum of Cu NWs coated with pluronic shows peaks at 1433, 1614, and 2864 cm^{-1} corresponding to the $-CH_3$, —OH, and —CH stretching modes, respectively, and confirming the coating of pluronic F-127 on the Cu NWs. In comparison to the Cu NWs coated with pluronic, the Cu@ZIF-8 NWs exhibit additional peaks. In the case of Cu@ZIF-8 NWs, the absorption peaks at 693, 761, 1144, and 1308 cm^{-1} can be attributed to the presence of ZIF-8.

The stability of Cu NWs and core-shell Cu@ZIF-8 NWs was assessed by SEM and XRD, which showed nanostructures were stable over 90 days' storage at ≈25 °C. The SEM image of the sample (Figure S7a, Supporting Information) revealed that the structure of Cu@ZIF-8 NWs was intact 90 days after its synthesis and storage in ethanol. No dramatic changes in the peak intensities or positions were evident in the XRD pattern of a sample stored for 90 days as a dry powder in air, though there is evidence of a faint peak near 36.46° that could be attributed to traces of copper oxides (Figure S7b, Supporting Information).

2.2. Characterization of Cu@ZIF-8 NW Functionalized Filter Media

The prepared Cu@ZIF-8 NWs were used to functionalize polypropylene based MERV15 filter material (three layer) using a simple dip-coating technique. To test the effect on filtration efficiency and other properties of filter media, four different concentrations of Cu@ZIF-8 NWs (0.1,0.25,0.5, and 1 mg mL^{-1}) were dispersed in ethanol to prepare four samples, hereafter labeled S2, S3, S4, and S5 (Figure S7a,b, Supporting Information). Moreover, to study the effect of solvent (ethanol) treatment alone, one sample (S1) was treated in ethanol and dried before testing and one untreated sample (S0) was used as a control. SEM (**Figure 3**a–d) was employed to analyze the prepared samples with varying concentrations of Cu@ZIF-8 NWs, confirming that Cu@ZIF-8 NWs were attached to the fibers of the filter media fairly uniformly. With increasing nanowire concentration, small aggregates were evident, as shown in the SEM image of a sample dipped in 1 mg mL^{-1} Cu@ZIF-8 NWs. Such high coverage may be important, as antimicrobial activity will presumably require direct contact of collected droplets with the Cu@ZIF-8 NWs.

The filtration efficiency of the prepared samples was evaluated to study the effect of Cu@ZIF-8 functionalization on the filtration media. **Figure 4**a presents the filtration efficiencies of the prepared samples. The bare untreated filter material (S0) has an efficiency of 72% for particles of size 0.3 µm. This

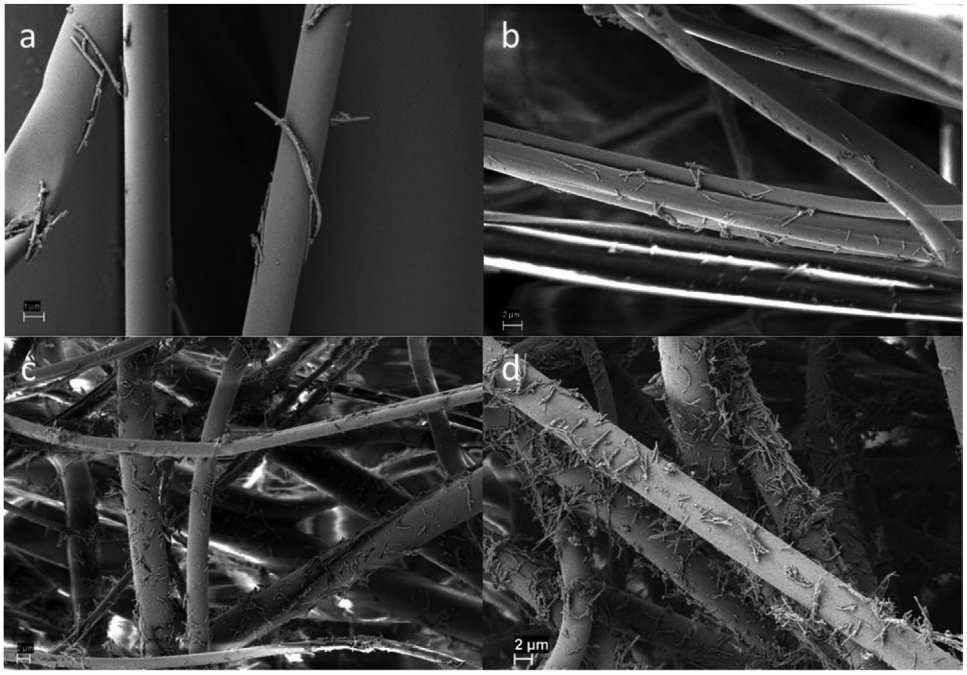

Figure 3. SEM images of face mask filter coated by dipping in dispersions of a) 0.1 mg mL^{-1}, b) 0.25 mg mL^{-1}, c) 0.5 mg mL^{-1}, and d) 1 mg mL^{-1} Cu@ZIF-8 NWs

efficiency is lower than that of N95 face masks which can capture 0.3 µm size aerosol particles with an efficiency of 97.5% in the same test. However, we note that our sample comprises a single layer filtration media sandwiched between two support layers and has lower pressure drop compared to N95 media due to its lower thickness. A two-layer version of such filter media can reach ≈95% efficiency for 0.3 micron particles, with comparable pressure drop to N95 media, as shown in Table S2, Supporting Information.

Filtration efficiency at 0.3 microns dropped drastically to 38.1% upon treating the sample (S1) with ethanol and drying before testing. This drop in filtration efficiency on treating face masks with disinfectants such as ethanol is possibly due to the loss of charges on the surface of polypropylene filter media, as previously reported by others.[45,46] Note, however, that the observed pressure drops (Table S2, Supporting Information) across the ethanol-treated and untreated filter media were identical, supporting the hypothesis that the observed loss the efficiency is due to the loss of static charges associated with the filter media and not a change in structure (swelling or deformation) of the media. Similar observations were recently reported by Liao and coworkers[5] where they observed a 80% drop in efficiency of N95 face masks upon treatment with 75% ethanolic solution with the pressure drop remaining constant. This drop in filtration efficiency can be restored using methods such as triboelectric charging,[47] and vacuum filtration.[48] We report a similar observation, when samples treated in 75% ethanolic nanocomposite solutions of varying concentrations were

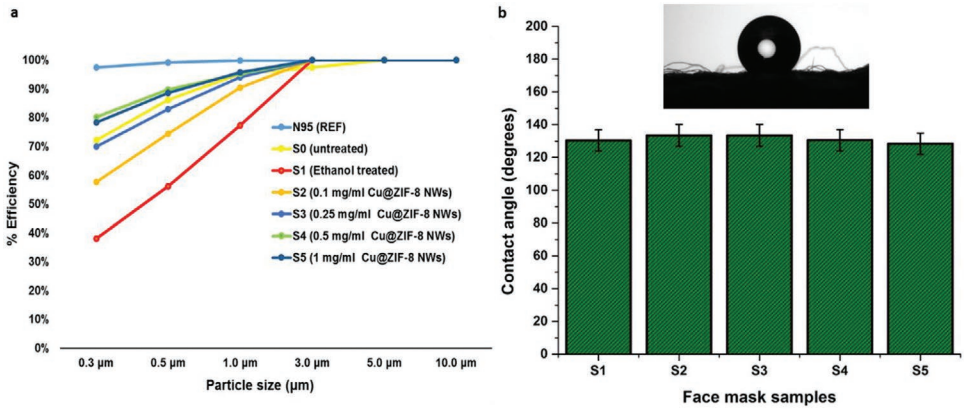

Figure 4. a) Filtration efficiency versus particle size for the Cu@ZIF-8 NW functionalized face mask materials. b) Water contact angle data for the face mask samples. Inset showing water droplet image on the untreated face mask material. The error bars are standard deviations based on three tests.

dried overnight in a vacuum oven, the filtration efficiency was restored closer to the initial value for bare untreated filter media. We also observed that on increasing the concentration of Cu@ZIF-8 NWs beyond 0.25 mg mL^{-1}, the filtration efficiency surpassed the efficiency of bare filter media. This increase in efficiency could be attributed to two factors. First, with increasing concentration of Cu@ZIF-8 NWs, the surface roughness of the filter media increases which in turn provides more surface area for capture of smaller aerosol particles. Second, the Cu@ZIF-8 NWs may impart a net surface charge due to the presence of ZIF-8, which is known to carry a net charge on its surface. Surface charge is an important factor in filtration efficiency.[48] The average zeta potential of Cu@ZIF-8 NWs measured in DI water at neutral pH was 6.54 mV, but the surface charge under dry conditions is likely different. The pressure drop increased slightly upon functionalization with Cu@ZIF-8 NWs. For 1 CFM flowrate, the pressure drop decreased from 0.29 (in W.C) for untreated filter media to 0.22 (in W.C) for ethanol treated media, then increased with Cu@ZIF-8 NW loading to 0.3 (in W.C) at the highest loading (Table S2, Supporting Information). In all cases, the pressure drop was much lower than typical N95 filter media tested for comparison (0.54 in W.C.). Increasing the flow rate to 3 CFM roughly tripled the pressure drops, indicating approximately linear dependence of pressure drop on flow rate for flows representative of mask applications.

The filter media that we have used is made up of melt-blown polypropylene, which is an inherently hydrophobic polymer. Hydrophobicity of filter media for face masks is an important contributing factor to their lifetime as well as their antibacterial and antiviral activity. Most respiratory disease viruses such as H1N1 and SARS-CoV-2 spread through respiratory droplets and fine aerosol particles generated by evaporation of respiratory droplets. The hydrophobic nature of the filter media imparts limited self-cleaning and antifouling properties to the face masks.[16,49] To confirm whether functionalization of Cu@ZIF-8 NWs affects the hydrophobicity of the face mask materials, water contact angle measurements for the samples (S1 to S5) were carried out. The untreated filter media (S1) had a static water contact angle of 133.5°. Functionalization of Cu@ZIF-8 NWs had little effect on the hydrophobicity, with a water contact angle of 128.4° for the sample dipped in 1 mg mL^{-1} solution. Figure 4b summarizes the results for static water contact angle of all five samples. Figure 4 (inset) presents an optical image of a water droplet on the surface of untreated filter media. The hydrophobicity of the media is maintained even after Cu@ZIF-8 NWs functionalization.

To determine if the Cu@ZIF-8 NW functionalized filter media sheds particles during filtration, we performed an experiment with a TSI Model 3010 condensation particle counter, in the arrangement shown in Figure S9b, Supporting Information. This counter detects particles down to about 10 nm diameter, and would therefore detect any Cu@ZIF-8 NWs shed from the filter media. A nominal reading from 1600–2000 particles/cm^3 was observed on the particle counter upon sampling room air during the day. We then attached a cartridge filter (P100 respirator cartridge in a custom holder) to our particle counter and observed a reading of zero particles/cm^3. Cu@ZIF-8 (1 mg mL^{-1}) loaded filter media was then placed in a filter holder between the cartridge filter and the particle counter. The sampling flow was 1 lpm through a 25 mm diameter circle of the treated filter medium. Any particles lost during the filtration process would appear on the particle counter. The zero particle count was maintained with the treated filter media in place. This demonstrates negligible loss of Cu@ZIF-8 NWs from the treated filter media.

2.3. Biocompatibility Testing of Nanomaterials

Although filtration testing of the mask materials showed no evidence of their release from the mask material, possible human exposure to the materials is an obvious potential concern. Any Cu@ZIF-8 NWs released from a treated mask could potentially be deposited in the oral cavity, throat, or lungs. Thus, we studied the likely biocompatibility of the material with such tissues. Note that in the envisioned application, the effective concentration to which microbes in collected exhaled droplets are exposed would be much higher than any concentration to which human cells might conceivably be exposed.

The MTT assay was carried out to probe dose-dependent and time-dependent cytotoxicity of Cu NWs, ZIF-8, and Cu@ZIF-8 NWs (0, 5, 10, 20, 40, 50, 80, 100, 160, 250, 500, 750, and 1000 μg mL^{-1}) toward A549 adenocarcinomic human alveolar basal epithelial cells (2 or 24 h exposure), human gingival epithelial-like (KB cells) and primary gingival fibroblasts (4 or 24 h exposure). For all cell types tested (Figures S10–S12, Supporting Information), the results showed that the cytotoxicity of Cu@ZIF-8 NWs was lower than that of uncoated CuNWs, which we attribute to sustained and controlled release of copper ions, rather than burst release. The IC50 of Cu@ZIF-8 NWs for A549 cells was found to be ≈88 μg mL^{-1}, which is 1.6-fold higher than that of Cu NWs (IC50 55 μg mL^{-1}). Time-dependent MTT assays were also performed to probe the cytotoxic effect of slow release of copper ions from Cu@ZIF-8 NWs. The result indicates increased cytotoxicity with time, particularly for higher exposure concentrations. This in vitro cytotoxicity measurement is consistent with the slow release of copper ions from Cu@ZIF-8 NWs, leading to sustained and time-dependent cytotoxicity.

2.4. ROS Imaging of Cells Treated with Cu@ZIF-8 NWs Functionalized Filter Media

For the A549 cells, we further studied the cellular response to exposure to the Cu@ZIF-8 NWs. Inflammation is a defensive immune response that is conferred by a host against foreign pathogens. The innate immune system on encountering pathogens elicits an acute inflammatory response that is accompanied by systemic vasodilation, vascular leakage, and leukocyte emigration. Such a measured response is advantageous to the organism, but if the response is unregulated then it results in inflammation and disease. Acute inflammatory response results in secretion of various cytokines. ROS are key signaling molecules that play an important role in the progression of inflammatory disorders. Production of ROS is central to the progression of inflammatory response. The ROS are produced by cells that are involved in the host-defense response and enhanced ROS generation at the site of inflammation causing tissue injury.

ROS act as both a signaling molecule and a mediator of inflammation. The concept of chronic or prolonged ROS production is considered central to the progression of inflammatory response. Ambient levels of ROS are important for homeostasis of cells; whereas increased ROS results in killing pathogens. The A549 lung epithelial cells treated with Cu@ZIF-8 functionalized mask filters showed sustained and increased ROS production at higher concentration (Figure S13, Supporting Information), which indicates that the nanoformulation induced increased inflammatory response in these cells. The nanoformulation may trigger antioxidant machinery of the cell.

2.5. Anti-Inflammatory Properties of Cu@ZIF-8 NWs Functionalized Filter Media

A549 cells were treated with 0.1, 0.25, and 0.5 mg mL^{-1} concentrations of Cu@ZIF-8 NWs for 24 h followed by extraction of RNA, conversion to cDNA and quantitation of gene expression levels by qPCR of pro-inflammatory cytokines, TNF-a, IL-8, and SOD1, which regulate oxidative stress. Cu@ZIF-8 NWs treatment resulted in a significant decrease in the gene expression of IL-8 by 78% (TAI = 0.21 ± 0.035; $p < 0.01$), 85% (TAI = 0.15 ± 0.029; $p < 0.01$), and 88% (TAI = 0.12 ± 0.017; $p < 0.01$) at 0.1, 0.25, and 0.5 mg mL^{-1}, respectively, as compared to the untreated control (TAI = 1.0 ± 0.015). Cu@ZIF-8 NWs treatment also resulted in a significant decrease in the expression of TNF-α by 61% (TAI = 0.39 ± 0.06; $p < 0.05$), 53% (TAI = 0.47 ± 0.041; $p < 0.05$), and 90% (TAI = 0.12 ± 0.011; $p < 0.01$) at 0.1, 0.25, and 0.5 mg mL^{-1}, respectively as compared to the untreated control (TAI = 1.0 ± 0.02). Both responses demonstrate the anti-inflammatory effects of Cu@ZIF-8 NWs (Figure S14, Supporting Information). Additionally, Cu@ZIF-8 NWs can inhibit cell signaling pathways triggered by pro-inflammatory cytokines (TNF-α and IL-8) and modulate numerous signaling molecules that may contribute to the potential anti-viral and anti-bacterial effects, under conditions in which the Cu@ZIF-8 NWs contact infected human cells.

Our results also showed a significant change in oxidative stress on treatment with Cu@ZIF-8 NWs, as reflected by a decrease in the gene expression level of SOD1. Our data (Figure S12, Supporting Information) show that Cu@ZIF-8 NW treatment resulted in a significant decrease in the gene expression of SOD1 by 30% (TAI = 0.70 ± 0.061; $p < 0.05$), 26% (TAI = 0.74 ± 0.03; $p < 0.05$), and 41% (TAI = 0.59 ± 0.02; $p < 0.05$) at 0.1, 0.25, and 0.5 mg mL^{-1}, respectively as compared to the untreated control (TAI = 1.0 ± 0.003). SOD1 is pivotal in ROS release during oxidative stress. We observed that treatment of A549 cells with Cu@ZIF-8 NWs resulted in a decrease in SOD1 gene expression.

2.6. Antibacterial Activity

Although hydrophobicity promotes reusability and provides some protection against microbes spreading through droplets, viable viruses and bacteria may remain on the surface of the mask. To confirm biocidal properties of Cu@ZIF-8 NWs and sustained release of Cu ions, we first considered antibacterial activity, as assays of antibacterial activity are much more straightforward and accessible than assays of antiviral activity, particularly for pathogenic viruses.

For testing antibacterial activity, strains of *S. mutans* and *E. coli* were chosen as model organisms. The relationship between the Cu@ZIF-8 NW concentration and bacterial growth was observed by measuring optical density at 600 nm. As shown in **Figure 5**a,b, addition of Cu@ZIF-8 strongly inhibits the growth of both types of bacteria at five different concentrations, that is, 25, 75, 150, 250, and 375 μg mL^{-1}. The average diameter of Cu@ZIF-8 NWs used here is 80 nm. Particle size can have a great impact on antibacterial activity. In many cases, the smaller the particle size, the higher the antibacterial activity. This has been attributed to the possibility that smaller particles may more easily penetrate through the bacterial cell wall and cell membrane as compared to larger ones.[17,50,51] To test the hypothesis that well-controlled core-shell structures can be advantageous for antibacterial applications, separate Cu NWs, and ZIF-8 nanoparticles were also tested for their antibacterial effect. The Cu@ZIF-8 nanocomposite exhibited greater antibacterial activity than either ZIF-8 or Cu NWs alone, against both bacterial strains, as shown in Figure 5c. Concentrations above 375 μg mL^{-1} of Cu@ZIF-8 did not show any increase in efficacy. This might be because of the aggregation due to increased number of particles which results in decreased surface area.[52]

After 26 h, Cu@ZIF-8 gave 91% inhibition of *E. coli* and 86% inhibition of *S. mutans* bacterial growth at a concentration of 375 μg mL^{-1}. At the same concentration, Cu NWs and ZIF-8 nanoparticles exhibited lower antibacterial activity for *E. coli* (Cu NWs: 36% inhibition and ZIF-8: 14% inhibition) and *S. mutans* (Cu NWs: 36% inhibition and ZIF-8: 14% inhibition). Cu@ZIF-8 NWs thus provide superior antibacterial effect. The presence of the ZIF-8 layer on Cu NWs not only provides the sustained release of Cu^{2+} from Cu NWs but also improves the stability of Cu NWs, slows oxidation of Cu NWs and reduces their aggregation. The gradual degradation of the Cu@ZIF-8 NWs and the release of Zn^{2+} ions and Cu^{2+} ions can physically disrupt the bacterial cell wall. We attribute the excellent antibacterial activity of Cu@ZIF-8 NWs to the synergistic effects of Cu core and ZIF-8 shell.

The modification of Cu NWs with ZIF-8 coating and pluronic slowed the release of Cu^{2+} ions at 37 °C in culture media over a period 96 h. Cu@ZIF-8 NWs released 18% and 35% of their Cu^{2+} within 24 and 48 h, respectively. The pluronic-coated Cu NWs also showed similar controlled release of 26% and 46% of Cu^{2+} within 24 and 48 h, respectively, and we attribute this slow release to the pluronic coating (Figure 5d). Without pluronic coating, the Cu NWs were not dispersible in phosphate buffered saline (PBS) buffer. Thus, release experiments could not be conducted for that case. The sustained release of Cu^{2+} reflects the improved stability of Cu@ZIF-8 NWs in culture media. The amount of Cu^{2+} ions in both Cu NWs and Cu@ZIF-8 NWs was the same for this comparison. The zinc ion release from Cu@ZIF-8 NWs appeared to saturate after 24 h, while Cu^{2+} ion release continued.

We also performed a study of copper ion release from CuNWs and Cu@ZIF-8 NWs in brain heart infusion (BHI) media, using UV–Vis spectroscopy to monitor ion concentrations. In this case, the difference in rate of copper ion release between CuNWs

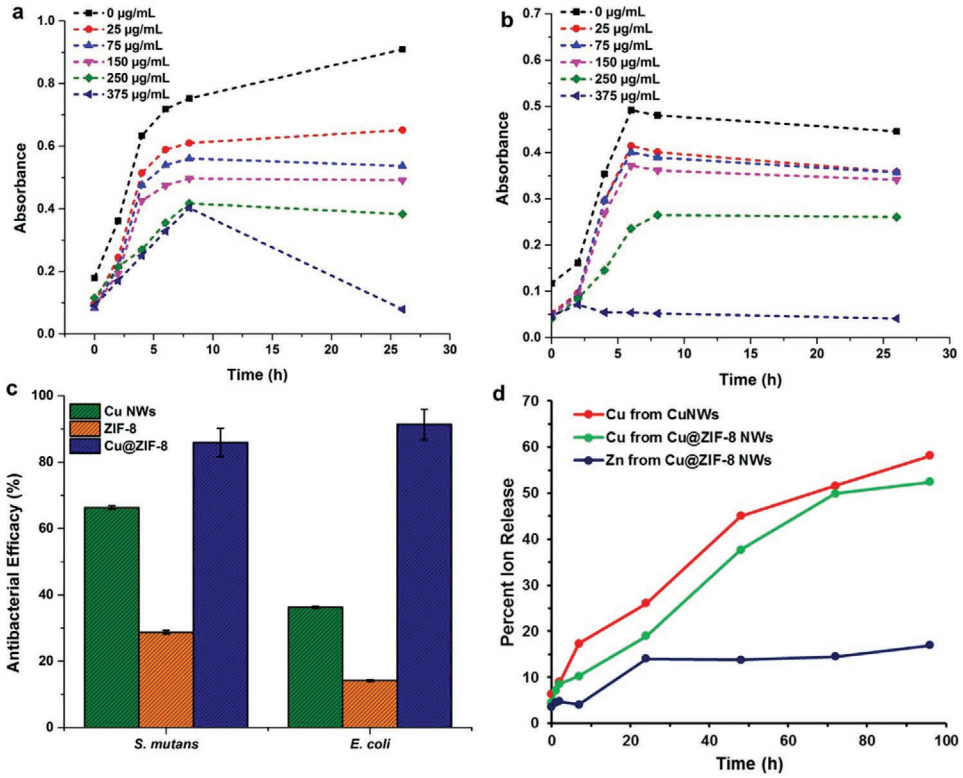

Figure 5. Growth curves of a) *E. coli* and b) *S. mutans* inoculated with different concentrations of Cu@ZIF-8 NWs. c) Antimicrobial efficacy (percent reduction in OD at 600 nm after 26 h) of Cu NWs, ZIF-8 and Cu@ZIF-8 core-shell heterostructure nanowires against *S. mutans* and *E. coli* bacterial strains at concentrations of 375 μg mL^{-1} (A representative experiment is shown. Error bars represent SEM of three technical replicates). d) Release profile of copper and zinc ions from Cu NWs and Cu@ZIF-8 NWs in cell media ($n = 3$. $p < 0.05$).

and Cu@ZIF-8 NWs is more distinct. However, in this analysis we do not have absolute quantification, and treat the amount released after 48 h as 100% release. This method also does not provide information on zinc ion release (Figure S15, Supporting Information).

The unique composition and structure of Cu@ZIF-8 NWs is responsible for their antibacterial activity. Cu@ZIF-8 NWs show release of copper and zinc ions in contrast to Cu NWs alone, which oxidize and aggregate in biological media. The antibacterial activity (**Figure 6**b) may begin as soon as the Cu@ZIF-8 NWs start degrading and releasing copper and zinc ions which eventually interact with the bacterial cell membrane and degrade it, disrupt the metabolism of the cell, cause oxidative stress due to the generation of ROS, and hence interfere with the physiological function of the cell.[53] SEM images of bacteria incubated on untreated filter media display intact structure (Figure 6c) while bacteria on Cu@ZIF-8 NW treated filter media (Figure 6d) demonstrate deformed surface structure suggesting that Cu@ZIF-8 NWs may cause collapse and disruption of *E. coli* cell membranes.

2.7. Antibacterial Performance of Cu@ZIF-8 NWs Functionalized Filter Media

As a further proof-of-concept demonstration, we determined the antibacterial effects of Cu@ZIF-8 NWs functionalized filter media under exposure conditions relevant to use in face masks. The self-cleaning potential of Cu@ZIF-8 NWs functionalized filter media was determined by comparing with untreated (S0) and ethanol-treated (S1) filter media. As shown in Figure S17, Supporting Information, samples, S0, S1, S2, S3, S4, and S5 were exposed to bacteria-laden aerosols generated from *E. coli* suspensions for 30 min. We observed that subsequent colony formation (growth) of bacteria from both the filter media samples themselves and extracts from the media dropped upon increasing the concentration of Cu@ZIF-8 NWs applied to the filter media from 0.1 to 1 mg mL^{-1}. Negligible growth of colonies on the filter media functionalized with 1 mg mL^{-1} of Cu@ZIF-8 was observed (S5). We also observed the maximum growth of *E. coli* bacterial colonies on agar plates for untreated and ethanol-treated filter media, suggesting that the base filter media does not exhibit significant antibacterial effects for these conditions. In contrast, the Cu@ZIF-8 functionalized filter media possesses excellent antibacterial effects, as evidenced by the dramatic decline in bacterial colonies upon increasing the concentration of Cu@ZIF-8 NWs used in treating the media, from 0.1 to 1 mg mL^{-1}.

2.8. Antiviral Activity

The SARS-CoV-2 coronavirus genetic material is composed of ≈30 000 nucleotides. It has four structural proteins,

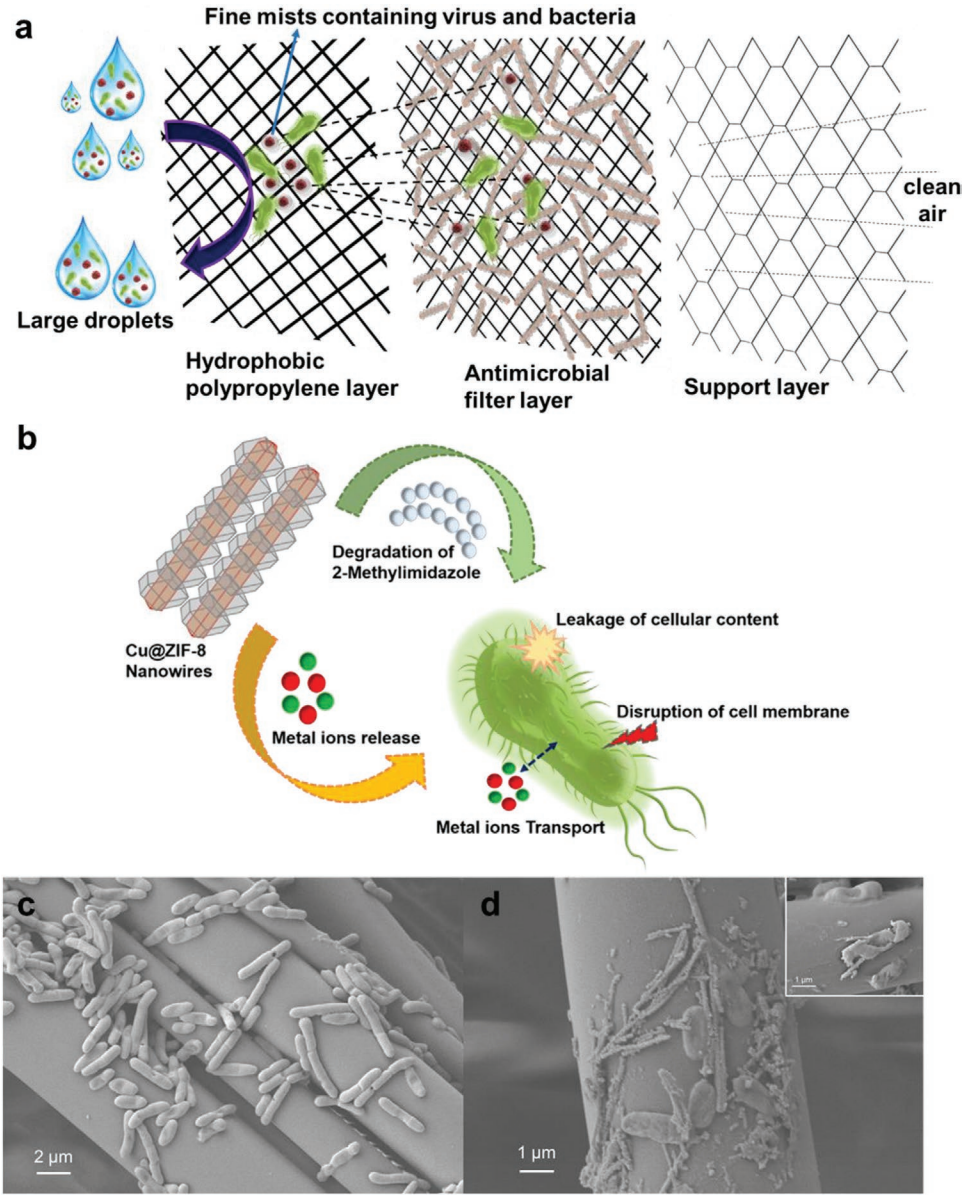

Figure 6. a) Schematic of Cu@ZIF-8 functionalized filter media and its filtration mechanism against microbe-containing aerosol droplets. b) The probable antibacterial mechanism shown by core-shell Cu@ZIF-8 NWs. SEM images of c) bare filter media containing *E. coli*. d) Cu@ZIF-8 NWs loaded filter media showing deformation of the *E. coli* membrane suggesting cell death.

nucleocapsid (N) protein, membrane (M) protein, spike (S) protein, and envelop (E) protein and several other non-structural proteins (**Figure 7**a). The capsid consists of a protein shell, with a nuclear capsid or N-protein inside the capsid bonded to single stranded RNA. This genome hijacks cells to produce a large number of viral copies. The genome is responsible for replication and transcription. The Envelop (E)-protein is composed of several amino acids ≈76 to 109 and some components of virus particles which ultimately aid in assembly of the virus and have an important role in host-virus cell interaction and host cell membrane permeation. Therefore, for the testing of anti-viral drugs, N or E protein can be used as the target.[54]

We evaluated the effect of Cu@ZIF-8 NWs on SARS COV-2 infection in vitro compared with Remdesivir (10 μM; positive control). We calculated the % inhibition of virus replication based on the fold change in the Ct value in Cu@ZIF-8 NW treated cells compared to the control. We observed a significant decrease in Ct values of N and E gene sequences, that is, 54.6% and 37.6%, respectively along with a cell viability of 99% at 48 h post infection for cells incubated with 1 μg Cu@ZIF-8 NWs per well (Figure 7b,c, Supporting Information). These findings demonstrate the anti-viral properties of Cu@ZIF-8 NWs against SARS-CoV-2, even at extremely low, drug-like concentrations (<10 ppm by mass) in the media. Effective concentrations in an exhaled droplet deposited on treated mask material are uncertain, but are likely to be orders of magnitude higher. For example, a 1 μm-diameter droplet with a 100 nm-diameter Cu@ZIF-8 NW passing through it would have a nominal

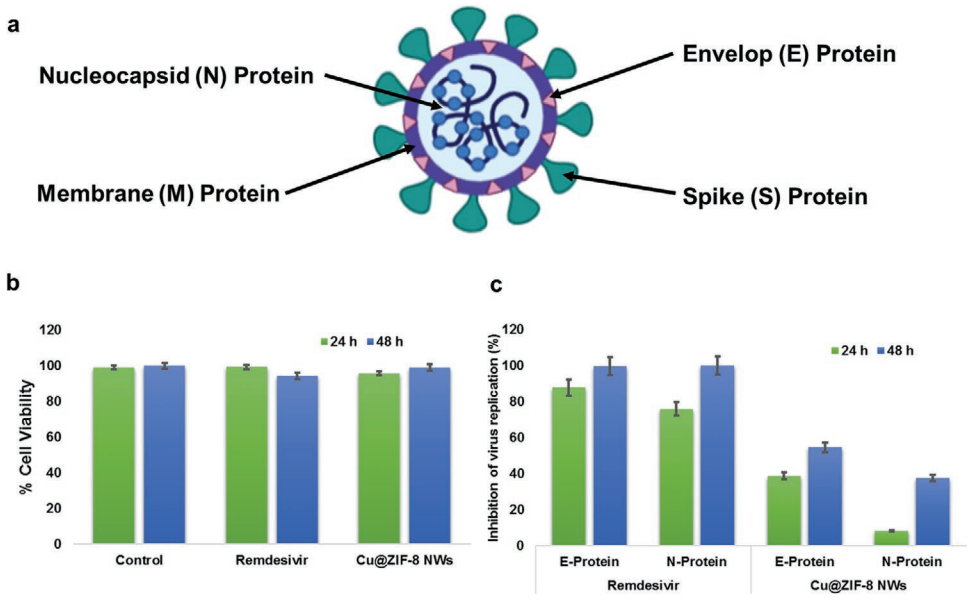

Figure 7. a) Schematic of SARS-CoV-2 showing S, N, E, and M structural proteins; b) Bar graph showing cytotoxicity of Cu@ZIF-8 NWs and Remdesivir on Vero E6 cells; c) Bar Graph showing antiviral effects of Cu@ZIF-8 NWs and Remdesivir at 24 h and 48 h post infection.

Cu@ZIF-8 NW concentration of about 50 000 ppm, and a 5 µm-diameter droplet with a single 100 nm-diameter Cu@ZIF-8 NW passing through it would have a concentration of about 2000 ppm. While such concentrations are not appropriate for use in an assay developed for testing antiviral drugs, one would clearly expect much greater inhibition at such concentrations. Future studies will be required, and are planned, to address antiviral activity upon exposure of the treated mask material to virus-laden aerosols, similar to the aerosol exposure experiments with bacteria described in Section 2.7. While these are more directly relevant to the end application, they are also more difficult to safely conduct.

The Cu@ZIF-8 NW functionalized filters, when used in face masks, may provide a continuous self-sanitizing effect by sustained release of copper and zinc ions. The microbes released by the person wearing the face mask will be neutralized by the release of copper and zinc ions, and this action should be further accelerated by the moisture in the exhaled breath, cough, or sneeze which may allow transport of ions to microbes that are not in direct contact with the nanocomposite; droplets and condensation will be in direct contact with the nanocomposite and allow transport of copper and zinc ions. Moreover, a recent study reports that the novel coronaviruses are not viable on copper surfaces for more than 4 h.[21] Hence, any coronavirus coming in contact with the face mask functionalized with Cu@ZIF-8 NWs should eventually be deactivated, improving the safety of reusing the face mask and reducing the need for other disinfection procedures.

3. Conclusion

In conclusion, we report a simple strategy for synthesis of novel thin Cu@ZIF-8 NW nanocomposites, and demonstrate that these materials can be easily coated on the surface of the fibers in filtration media like that used in medical-grade face masks using a simple dip-coating technique. The filtration efficiency of the Cu@ZIF-8 NW-functionalized filter media was found to be directly correlated to the concentration of the nanocomposite solution into which it was dipped. A slight decrease in hydrophobicity of the functionalized polypropylene fibers was observed. However, the surface still remained highly hydrophobic, which is essential to limit accumulation of incoming moisture. If microbes reach and adhere to the surface of the face mask fibers, they will be inactivated by ions released from the Cu@ZIF-8 NWs. Compared to bare Cu NWs or ZIF-8, the Cu@ZIF-8 NWs shows enhanced antibacterial activity, likely due to simultaneous release of Cu and Zn ions. Cu@ZIF-8 NWs exhibit lower cytotoxicity than bare CuNWs, and reduced the excess synthesis of pro-inflammatory cytokines and ROS compared to bare CuNWs. Moreover, the formed nanocomposites are thermally and chemically stable, making the treated masks durable for multiple wearings. The simple low cost-procedure reported here can be used to functionalize any face mask fiber, imparting biocidal and self-sanitizing properties.

4. Experimental Section

Chemicals: Copper(II) chloride dihydrate ($CuCl_2.2H_2O$, ≥99%, Alfa Aesar), oleylamine (OAm, 70%, technical grade, Sigma-Aldrich), oleic acid (OA, Fisher Chemical), L-ascorbic acid (AA, 99%, Sigma-Aldrich), zinc acetate ($Zn(OAc)_2$, 99.99%, Sigma-Aldrich), 2-methylimidazole (MI, TCI chemicals), ethanol (200 proof, DECON Laboratories), hexane (99%, ACS Reagent, ACROS Organics).

Cell Culture: Archived primary human gingival fibroblasts (HGF) from healthy donors or the gingival epithelial carcinoma-like cell line KB, and A549—a human epithelial lung carcinoma cell line (Cat # ATCC CCL-185)—were used as representative oral cell types and pulmonary lung cell types, respectively. HGF cells were grown in DMEM + 10% fetal bovine serum (FBS) and KB cells grown in αMEM + 10% FBS and

routinely passaged using 0.25% Trypsin/EDTA. A549 cells were grown in ATCC-formulated F-12K Medium (Cat#. 30–2004) and complete growth medium, which includes addition of the following components to the base medium: Penicillin Streptomycin solution 1% and 10% FBS.

Copper Nanowire Synthesis: Ultra-thin Cu NWs were prepared by an aqueous one-pot synthesis route. In a typical synthesis, 675 mg of $CuCl_2.2H_2O$ was first dissolved in 380 mL of DI water in a glass bottle by stirring at ambient temperature. 5 mL of OAm, 100 µL of OA, and 15 mL of ethanol were sonicated in a 20 mL glass vial for 10 min then added into the continuously stirred aqueous copper salt solution. The copper solution changed from its initial blue color to greenish-blue upon the addition of ethanolic OAm. The resulting solution was stirred continuously for another one hour before adding 500 mg of AA. The mixture was stirred for another 10 min then placed in an oven at 85 °C for 12 h. After that, the glass bottle was taken out and left in air to cool to room temperature. As Cu NWs are formed in the solution, they settle to the bottom of the bottle, so 90% of the mixture volume was first decanted to obtain concentrated Cu NWs. The remaining 10% contained a majority of the Cu NWs and was centrifuged at 6000 rpm for 10 min, the supernatant was discarded, a mixture of ethanol and hexane (1:1 volume ratio) was added, and the sample was centrifuged again at 6000 RPM for 10 min. The obtained thin Cu NWs were finally dispersed in ethanol for further use.

Synthesis of Cu@ZIF-8 NWs: For stabilization of Cu NWs, 450 mg of Cu NWs and 5 g of Pluronic F-127 were added to 450 mL of ethanol and water (1:1) and stirred for 24 h. Then, the reaction mixture was centrifuged at 6000 rpm for 10 min and washed with ethanol thrice. For a uniform coating of ZIF-8 over the CuNWs, a slightly modified procedure for ZIF-8 synthesis was followed.[55] The pluronic-stabilized Cu NWs were dispersed in 350 mL of ethanol with 0.4675 g of zinc acetate dihydrate and stirred for another one hour to allow adsorption of zinc ions on the Cu NWs. Then, 1.845 g of 2-methylimidazole was dissolved in 100 mL of ethanol then added into the above solution with continued stirring for 5 or 15 min. After 5 min, beaded Cu@ZIF-8 NWs were formed, and after 15 min, core-shell Cu@ZIF-8 heterostructures NWs were formed. The obtained nanostructures were centrifuged at 10000 rpm for 10 min and washed with ethanol thrice, then dried overnight in a vacuum oven at 60 °C.

Characterization of Cu and Cu@ZIF-8 NWs: The size and morphology of the Cu and Cu@ZIF-8 NWs were investigated using a JEOL JEM-2010 TEM at an accelerating voltage of 200 kV. TEM grids (200-mesh copper with carbon support film) were prepared by dropping a dilute ethanolic dispersion of Cu NWs or Cu@ZIF-8 NWs onto them, followed by drying under ambient conditions. SEM images of samples were taken using a ZEISS Cross-beam Focused Ion Beam SEM. The Cu@ZIF-8 NW sample was coated with a thin layer of gold using a SPI-Module Sputter Coater system. The crystal structure of samples was studied using XRD analysis with a Rigaku Ultima IV diffractometer with Cu Kα X-ray source with a wavelength of 1.54 Å. Nitrogen adsorption-desorption isotherms, and the surface area of Cu@ZIF-8 NWs were analyzed using a Micromeritics Tri-Star II system with Micromeritics VacPrep 061 (sample degas system). The samples were degassed under vacuum at 150 °C for 4 h before taking their surface area measurement. The thermal stability of the samples was analyzed by TGA using a TA instruments SDT Q-600 under a nitrogen atmosphere. Attenuated total reflection FTIR spectra of CuNWs, ZIF-8, and Cu@ZIF-8 NWs were collected using a Bruker Vertex 70 spectrometer.

Preparation of Cu@ZIF-8 NW Functionalized Filter Media, Its Filtration Efficiency, and Contact Angle Measurements: A simple dip coating method was used to load Cu@ZIF-8 NWs onto fibrous filter media. First, a Cu@ZIF-8 NW dispersion in 75% ethanolic solution of the desired concentration was sonicated for half an hour. Samples of MERV-15 filter media (McMaster–Carr, part number 22905K63) were cut into 3×3 inch squares, dipped into the ethanolic dispersion of Cu@ZIF-8 of varying concentration, pulled out slowly by hand, and dried in a vacuum oven overnight before further characterization. A blank sample dipped in 200 proof ethanol was also prepared and used as a control.

The filtration efficiency of the filtration media was evaluated using a custom-built set-up, as shown in Figure S9a, Supporting Information. The set-up comprises a particle counter (Lighthouse 3100) to measure the aerosol both upstream and downstream of the filter, a filter housing of 2.25-inch diameter and 18.41 cm s^{-1} face velocity, a differential pressure sensor to measure the pressure drop across the filter, and finally a combination of flowmeter and vacuum pump. Pressure drop measurements were evaluated at flow rates of 1 and 3 CFM, corresponding to breathing rates at rest and moderate activity. Filtration efficiency measurements were made at 1 CFM flow rate. To get base readings, the bare filter media and ethanol-treated filter media were tested before nanocomposite functionalized filter media. A one-minute purge was provided before each reading to get rid of dust and contaminants before taking the final reading. Three readings of 10 s with an interval of 15 s between them were taken for both upstream (C_u) and downstream (C_d) particle concentrations. The filtration efficiency (*FE*) of the samples was calculated as:

$$FE = \frac{(C_u - C_d)}{C_u} \quad (1)$$

Water contact angles for the prepared samples were determined using a Ramé Hart goniometer (Model 190, Succasunna, NJ), and three measurements were taken for each sample.

SEM images of Cu@ZIF-8 NWs functionalized filter media were obtained after coating the samples with thin gold layer using a SPI-Module Sputter Coater System.

Release of Copper Ions from Cu NWs and Copper, Zinc Ions and 2-Methyl Imidazole Release from Cu@ZIF-8 NWs: The release of copper ions from Cu NWs and of both copper and zinc ions from Cu@ZIF-8 was studied using inductively coupled plasma-optical emission spectroscopy (ICP-OES) at time points 7, 24, 48, 72, and 96 h after dispersion in PBS buffer. In addition, the final Cu content in Cu@ZIF-8 was also analyzed by ICP-OES after the nanostructures were rinsed with ethanol thrice. 10 mg of Cu NWs or Cu@ZIF-8 was dispersed in 10 mL of 1% pluronic-containing cell media (free of Cu and Zn ions). The solution was incubated at 37 °C in a sealed vial for 4 days in a cell incubator. 1 mL aliquots were taken at various time points and filtered to estimate the release of copper and zinc ions, and an equal amount of fresh cell media was added to both samples. The filtered supernatant was diluted ten times with an acidic solution for the analysis. The actual concentration of the ions was determined based on a calibration curve constructed using certified standards. All the measurements were taken in triplicate for each sample.

The release of copper ions from CuNWs and Cu@ZIF-8 NWs in BHI media was studied using UV–Vis spectroscopy to monitor copper ion concentrations by noting the absorbance at 570 nm. For that, 10 mg of Cu NWs or Cu@ZIF-8 was dispersed in 10 mL of BHI media. The solution was incubated at 37 °C in a sealed vial for 3 days in a cell incubator. 1 mL aliquots were taken at various time points and filtered to estimate the release of copper, and an equal amount of fresh BHI media was added to both samples. The filtered supernatant was diluted three times with BHI for the analysis. Fresh BHI media was taken as a reference. All the measurements were taken in triplicate for each sample.

Concentration and Time-Dependent Copper-Induced Cytotoxicity: Time-dependent and concentration-dependent cytotoxicity of copper ions released from Cu NWs and Cu@ZIF-8 NWs were evaluated in vitro. Cell viability was measured by treating the A549 cells (10000 cells) in phenol free media, KB cells (5000 cells) or gingival fibroblasts (5000 cells) with different concentrations of Cu NWs, ZIF-8, and Cu@ZIF-8 NWs (0, 5, 10, 20, 40, 50, 80, 100, 160, 250, 500, 750, and 1000 µg mL^{-1}) for 2, 4, or 24 h. Cell viability was estimated using the Vybrant MTT Cell Proliferation Assay Kit (ThermoFisher Scientific). After incubating the nanoformulations containing cells for the mentioned time period at 37 °C, 10 µL of 12 mM MTT reagent (5 mg mL^{-1} in PBS) was added to each well and then further incubated for 2 h. The MTT reagent (water-soluble tetrazolium salt, WST-8) is reduced by the dehydrogenase activity in viable cells to give a yellow formazan dye soluble in the tissue culture media. The amount of the formazan dye generated by the dehydrogenase activity in cells is directly proportional

to the number of living cells. After that, 100 µL of SDS-HCl solution (A549 cells) or 200 µL DMSO (KB and fibroblast cells) was added to each well and mixed thoroughly using the pipette. The microplate was further incubated at 37 °C for 1 h in a humidified chamber. The optical density of the microplate was monitored at 570 nm using a plate reader.

For the Vero E6 cell line, the cytotoxicity assay is done in a 96-well plate format with three wells for each sample. 1×10^4 VeroE6 cells were plated per well and incubated at 37 °C overnight for monolayer formation. The next day, cells were incubated with the Cu@ZIF-8 NWs at the indicated concentration. The control cells were incubated with 1% ethanol. After 24 and 48 h incubation, cells were stained with Hoechst 33 342 and Sytox orange dye. Images were taken at 10×, 16 images per well, which covers 90% of the well area, using an ImageXpress Microconfocal imaging system (Molecular Devices). Hoechst 33 342 nucleic acid stain is a popular cell-permeant nuclear counter stain that emits blue fluorescence when bound to dsDNA. It stains both live and dead cells. Sytox orange dye stains nucleic acids in cells with compromised membranes. This stain is an indicator of cell death. First, the software counted the total number of cells in the Hoechst image. In the Sytox image, it counted, among Hoechst positive cells, those cells that were positive for Sytox.

Effect of Cu@ZIF-8 NWs on SOD1 Gene Expression as a Biomarker of Oxidative Stress: We evaluated the effect of Cu@ZIF-8 NW-media on superoxide dismutase (SOD1) gene expression in A549 cells. The SOD1 gene provides instructions for making an enzyme called superoxide dismutase, which is abundant in cells throughout the body. This enzyme attaches (binds) to molecules of copper and zinc to break down toxic, charged oxygen molecules called superoxide radicals. The molecules are byproducts of normal cell processes, and they must be broken down regularly to avoid damaging cells. A549 cells were treated with Cu@ZIF-8 NWs for 24 h, followed by RNA extraction, reverse transcription to cDNA, followed by quantitation of gene expression levels using real time qPCR. The cells without NP treatment served as the control.

RNA Extraction: Cytoplasmic RNA was extracted from A549 cells treated with Cu@ZIF-8 NW-functionalized filter-media treated, or untreated, by an acid guanidinium-thiocyanate-phenol-chloroform method using Trizol reagent (Invitrogen-Life Technologies, Carlsbad, CA). The amount of RNA was quantified using a Nano-Drop ND-1000 spectrophotometer (Nano-Drop, Wilmington, DE), and isolated RNA was stored at –80 °C until used.

Real Time qPCR: 100 ng of total RNA was used for the RT reaction (25 µL total volume) with the First Strand cDNA Synthesis Kit (GE Healthcare, Piscataway, NJ), according to the manufacturer's instructions. 1 µL of the resultant cDNA from the RT reaction was employed as the template in PCR reactions using specific pre-validated primers for TNF-α, IL-8, and SOD1 obtained from RealTimePrimers.com. Primers were diluted to a concentration of 10 µM in 10 mM Tris–HCl (pH 7.5) and 0.1 mM EDTA. The final primer concentration used in the PCR was 0.1 µM. PCR conditions were as follows: 95 °C for 3 min, followed by 24 cycles of 95 °C for 40 s, 58 °C for 30 s, and 72 °C for 1 min; the final extension was at 72 °C for 5 min. Gene expression was calculated using the comparative CT method. The threshold cycle (Ct) of each sample was determined, the relative level of a transcript (2ΔCt) was calculated by obtaining ΔCt (test Ct–GAPDH Ct), and transcript accumulation index (TAI) was calculated as TAI = $2-\Delta$CT (Livak KJ, Schmittgen TD 2001).

ROS Imaging: Cells (A549) were preincubated with six different concentrations of CuNWs or Cu@ZIF-8 (0, 20, 80, 100, 500, and 1000 µg mL^{-1}) for 24 h. After incubation, media was discarded and cells were washed with 1×PBS. After that, 10 µL of freshly prepared 8 µM carboxy-H2DCFDA dye was added. Cells were incubated for 30 min in a conventional incubator (37 °C). The buffer was discarded and 500 µL of pre-warmed phenol-free growth medium was added, followed by 500 µL of 1×PBS containing Trypan Blue 0.004% and incubation for 5 min. The cells were then washed twice with 1×PBS. Finally, 1×PBS with DAPI was added followed by 5 min incubation, and then cells were again washed with 1×PBS thrice. The fluorescence was detected over the emission range of 495/527 nm that is appropriate for green fluorescence. ROS generation levels were quantified with respect to a corresponding untreated control, based on the intensity of the fluorescent signal analyzed using the computer image analysis ImageJ software (National Institutes of Health, Bethesda, MA, USA).

Antibacterial Activity Assay: Bacteria, *S. mutans* ATCC 25 175 (gift from Dr. Stefan Ruhl, University at Buffalo) and *E. coli* DH5α, were streaked onto Brain Heart Infusion (BHI) (Sigma-Aldrich, St Louis, MO) agar plates and incubated overnight in at 37 °C. BHI broth (5 mL) was inoculated with bacteria and grown overnight at 37 °C. The overnight cultures were diluted 1:10 (3 mL into 27 mL fresh BHI) and 20 µL for culture was added to 200 µL of the various nanoparticle-BHI solutions in a 96-well flat-bottom plate and incubated at 37 °C. Growth was measured as optical density at 600 nm (OD_{600}), with 5 s shaking prior to measurement, using a spectrophotometer (FlexStation3 Multi-Mode Microplate Reader, Molecular Devices, San Jose, CA) every 2 h for 6 h and at 24 h. As these materials altered the color of BHI, for each nanoparticle material the, the OD_{600} of the solution alone was subtracted at each time point. Each concentration was evaluated in triplicate wells and the growth rate was plotted as the average OD_{600} over time.

For SEM images of bacteria on bare filter and Cu@ZIF-8 functionalized filter media, the samples were dipped in bacterial culture ($\approx5\times10^8$ CFUs/mL) for an hour and dried. They were then transferred to a Coplin jar with 2.5% glutaraldehyde (for 1 h at room temperature for fixation. Samples were then washed with DPBS for 10 min, and this process was repeated two more times. Samples were transferred to a jar containing 30% ethanol and incubated for 10 min, followed by a series of 10 min incubations in increasing percentages of ethanol: 50, 75, 85, 95, and twice in 100%. Finally, samples were removed and allowed to dry before applying a coat of hexamethyldisilazane (HMDS). SEM images of samples were taken after coating with a thin gold layer using SPI-Module Sputter Coater System.

Antibacterial Activity Assay for Aerosol Exposed Filter Media: To expose the treated filter media to bacteria under conditions more nearly replicating in-use conditions, an aerosol generator (3-jet Collison nebulizer, BGI, Inc.) was used along with a filter holder as shown in Figure S16, Supporting Information. Before starting the experiment, the setup was decontaminated by wiping thoroughly with 70% ethanol solution and placing it in a UV chamber within a biological safety cabinet for half an hour. Air pressure of 10 psi was passed through nebulizer containing ≈50 mL *E. coli* culture (1×10^5 CFUs/mL) to generate an aerosol comprising about 0.2 mL min^{-1} of liquid droplets in about 3 L min^{-1} of air. The generated aerosol was passed through the Cu@ZIF-8 NW-functionalized filter media (S0–S5) for 30 min to ensure complete exposure of the mask material. Six samples were exposed simultaneously, using a custom filter holder with six identical positions that directed the aerosol, in parallel, through a 0.5 inch circular region of each material. The filter media were then removed from the chamber and vortexed in 5 mL of 0.9% saline solution for 2 min. 100 µL of the vortexed saline was pipetted onto LB agar plates and incubated overnight at 37 °C. The Cu@ZIF-8 NWs functionalized filter media (S0–S5) exposed to bacterial aerosol solution were also placed on LB agar plates and incubated overnight at 37 °C to observe bacterial growth.

Antiviral Testing: The assay is done in a 96-well plate format with three wells for each sample. 1×10^4 VeroE6 cells were plated per well and incubated at 37 °C overnight for monolayer formation. The next day, cells were incubated with the Cu@ZIF-8 NWs at the indicated concentration. The control cells were incubated with 1% ethanol. The cells were infected with SARS-CoV-2 at a MOI of 0.01. After 24 and 48 h, viral RNA was extracted from 100 µL culture supernatant and subjected to qRT-PCR (in duplicate) where Ct values for N and E gene sequence were determined. Inhibition of virus replication is determined based on the fold change in the Ct value in treated cells compared to the control. Remdesivir was used as a positive control for viral inhibition.

Statistical Analysis: The data were analyzed using Prism 8.0 (GraphPad Software, La Jolla, CA). Results are expressed as mean ± SD. For comparisons between two groups, the Student's *t*-test was used. Statistical comparisons between more than two groups were done using an analysis of variance (ANOVA). A p value <0.05 was considered as a statistically significant difference.

Supporting Information

Supporting Information is available from the Wiley Online Library or from the author.

Acknowledgements

A.K. and A.S. contributed equally to this work. The authors thank the Department of Science and Technology (DST), Government of India, for providing the Indo-US Overseas fellowship for women in STEMM (WISTEMM). The authors also thank Xiaoyi Chen for assistance with contact angle measurement, Matt Malloy and Mike Garman of EWI, Inc. for assistance with filter testing, and Regional Centre for Biotechnology, Faridabad, India for performing SARS-CoV-2 antiviral testing. Biorender software was used in preparing Figure 7a.

Conflict of Interest

The authors declare no conflict of interest.

Keywords

antibacterial activity, copper nanowires, COVID-19, metal-organic frameworks, ZIF-8

Received: September 21, 2020
Revised: November 16, 2020
Published online: December 13, 2020

[1] E. Dong, H. Du, L. Gardner, *Lancet Infect. Dis.* **2020**, *20*, 533.
[2] *Rapid Expert Consultation on the Possibility of Bioaerosol Spread of SARS-CoV-2 for the COVID-19 Pandemic (1 April 2020)*, National Academies Press, Washington **2020**.
[3] R. Tellier, Y. Li, B. J. Cowling, J. W. Tang, *BMC Infect. Dis.* **2019**, *19*, 101.
[4] N. H. L. Leung, D. K. W. Chu, E. Y. C. Shiu, K. H. Chan, J. J. McDevitt, B. J. P. Hau, H. L. Yen, Y. Li, D. K. M. Ip, J. S. M. Peiris, W. H. Seto, G. M. Leung, D. K. Milton, B. J. Cowling, *Nat. Med.* **2020**, *26*, 676.
[5] L. Liao, W. Xiao, M. Zhao, X. Yu, H. Wang, Q. Wang, S. Chu, Y. Cui, *ACS Nano* **2020**, *14*, 6348.
[6] *Rapid Expert Consultation on the Effectiveness of Fabric Masks for the COVID-19 Pandemic (8 April 2020)*, National Academies Press, Washington **2020**.
[7] A. Konda, A. Prakash, G. A. Moss, M. Schmoldt, G. D. Grant, S. Guha, *ACS Nano* **2020**, *14*, 6339.
[8] C. Makison Booth, M. Clayton, B. Crook, J. M. Gawn, *J. Hosp. Infect.* **2013**, *84*, 22.
[9] Y. Li, P. Leung, L. Yao, Q. W. Song, E. Newton, *J. Hosp. Infect.* **2006**, *62*, 58.
[10] M. Haas, *US20080295843A1*, **2007**.
[11] C. B. Hiragond, A. S. Kshirsagar, V. V. Dhapte, T. Khanna, P. Joshi, P. V. More, *Vacuum* **2018**, *156*, 475.
[12] L. Tamayo, M. Azócar, M. Kogan, A. Riveros, M. Páez, *Mater. Sci. Eng., C* **2016**, *69*, 1391.
[13] M. Hashmi, S. Ullah, I. S. Kim, *Curr. Biotechnol.* **2019**, *1*, 1.
[14] E. Horváth, L. Rossi, C. Mercier, C. Lehmann, A. Sienkiewicz, L. Forró, *Adv. Funct. Mater.* **2020**, *30*, 2004615.
[15] L. Huang, S. Xu, Z. Wang, K. Xue, J. Su, Y. Song, S. Chen, C. Zhu, B. Z. Tang, R. Ye, *ACS Nano* **2020**, *14*, 12045.
[16] H. Zhong, Z. Zhu, J. Lin, C. F. Cheung, V. L. Lu, F. Yan, C. Y. Chan, G. Li, *ACS Nano* **2020**, *14*, 6213.
[17] Y. N. Slavin, J. Asnis, U. O. Häfeli, H. Bach, *J. Nanobiotechnol.* **2017**, *2*, 65.
[18] G. Borkow, J. Gabbay, *Curr. Chem. Biol.* **2009**, *3*, 272.
[19] M. S. Usman, M. E. El Zowalaty, K. Shameli, N. Zainuddin, M. Salama, N. A. Ibrahim, *Int. J. Nanomed.* **2013**, *8*, 4467.
[20] S. L. Warnes, Z. R. Little, C. W. Keevil, *mBio* **2015**, *6*, e01697.
[21] N. Van Doremalen, T. Bushmaker, D. H. Morris, M. G. Holbrook, A. Gamble, B. N. Williamson, A. Tamin, J. L. Harcourt, N. J. Thornburg, S. I. Gerber, J. O. Lloyd-Smith, E. De Wit, V. J. Munster, *N. Engl. J. Med.* **2020**, *382*, 1564.
[22] Y. Qi, J. Ye, S. Ren, J. Lv, S. Zhang, Y. Che, G. Ning, *J. Hazard. Mater.* **2020**, *387*, 121687.
[23] K. Jomova, M. Valko, *Toxicology* **2011**, *283*, 65.
[24] G. J. Brewer, *Chem. Res. Toxicol.* **2010**, *23*, 319.
[25] X. X. Xu, F. L. Nie, Y. B. Wang, J. X. Zhang, W. Zheng, L. Li, Y. F. Zheng, *Acta Biomater.* **2012**, *8*, 886.
[26] Z. Chen, H. Meng, G. Xing, C. Chen, Y. Zhao, G. Jia, T. Wang, H. Yuan, C. Ye, F. Zhao, Z. Chai, C. Zhu, X. Fang, B. Ma, L. Wan, *Toxicol. Lett.* **2006**, *163*, 109.
[27] N. Hanagata, F. Zhuang, S. Connolly, J. Li, N. Ogawa, M. Xu, *ACS Nano* **2011**, *5*, 9326.
[28] S. Pal, Y. K. Tak, J. M. Song, *Appl. Environ. Microbiol.* **2007**, *73*, 1712.
[29] A. Kumar, M. M. Mohammadi, M. T. Swihart, *Nanoscale* **2019**, *11*, 19058.
[30] C. Hwang, J. An, B. D. Choi, K. Kim, S. W. Jung, K. J. Baeg, M. G. Kim, K. M. Ok, J. Hong, *J. Mater. Chem. C* **2016**, *4*, 1441.
[31] R. Ramakrishnan, B. Bharaniraja, A. S. Aprem, *Contraception* **2015**, *92*, 585.
[32] J. Xiao, S. Chen, J. Yi, H. F. Zhang, G. A. Ameer, *Adv. Funct. Mater.* **2017**, *27*, 1604872.
[33] W. Lu, Z. Wei, Z. Y. Gu, T. F. Liu, J. Park, J. Park, J. Tian, M. Zhang, Q. Zhang, T. Gentle, M. Bosch, H. C. Zhou, *Chem. Soc. Rev.* **2014**, *43*, 5561.
[34] B. Li, H.-M. Wen, Y. Cui, W. Zhou, G. Qian, B. Chen, *Adv. Mater.* **2016**, *28*, 8819.
[35] D. Zou, D. Liu, J. Zhang, *Energy Environ. Mater.* **2018**, *1*, 209.
[36] B. Chen, Z. Yang, Y. Zhu, Y. Xia, *J. Mater. Chem. A* **2014**, *2*, 16811.
[37] S. Zhao, F. Han, J. Li, X. Meng, W. Huang, D. Cao, G. Zhang, R. Sun, C. P. Wong, *Small* **2018**, *14*, 1800047.
[38] Y. Wang, M. Zhao, Q. Zhao, Q. Li, H. Pang, *Nanoscale* **2018**, *10*, 15755.
[39] Y. F. Guo, W. J. Fang, J. R. Fu, Y. Wu, J. Zheng, G. Q. Gao, C. Chen, R. W. Yan, S. G. Huang, C. C. Wang, *Appl. Surf. Sci.* **2018**, *435*, 149.
[40] D. Zhang, P. Liu, S. Xiao, X. Qian, H. Zhang, M. Wen, Y. Kuwahara, K. Mori, H. Li, H. Yamashita, *Nanoscale* **2016**, *8*, 7749.
[41] Q. Li, S. Gong, H. Zhang, F. Huang, L. Zhang, S. Li, *Chem. Eng. J.* **2019**, *371*, 26.
[42] D. Wu, X. Zhang, J. Zhu, D. Cheng, *Eng. Sci.* **2018**, *2*, 49.
[43] A. M. Bodratti, P. Alexandridis, *J. Funct. Biomater.* **2018**, *9*, 11.
[44] Y. Hu, H. Kazemian, S. Rohani, Y. Huang, Y. Song, *Chem. Commun.* **2011**, *47*, 12694.
[45] H. Xiao, Y. Song, G. Chen, *J. Electrost.* **2014**, *72*, 311.
[46] A. L. Sanchez, J. A. Hubbard, J. G. Dellinger, B. L. Servantes, *Aerosol Sci. Technol.* **2013**, *47*, 606.
[47] M. Zhao, L. Liao, W. Xiao, X. Yu, H. Wang, Q. Wang, Y. L. Lin, F. S. Kilinc-Balci, A. Price, L. Chu, M. C. Chu, S. Chu, Y. Cui, *Nano Lett.* **2020**, *20*, 5544.
[48] A. I. Nazeeri, I. A. Hilburn, D.-A. Wu, K. A. Mohammed, D. Y. Badal, M. H. W. Chan, J. L. Kirschvink, *medRxiv* **2020**, 2020.04.12.20059709.
[49] N. El-Atab, N. Qaiser, H. Badghaish, S. F. Shaikh, M. M. Hussain, M. M. Hussain, *ACS Nano* **2020**, *14*, 7659.
[50] Y. Zhang, X. Zhang, J. Song, L. Jin, X. Wang, C. Quan, *Nanomaterials* **2019**, *9*, 1579.
[51] H. Nabipour, M. H. Sadr, N. Thomas, *New J. Chem.* **2016**, *40*, 238.
[52] A. Malik, M. Nath, S. Mohiyuddin, G. Packirisamy, *ACS Omega* **2018**, *3*, 8288.
[53] M. Shen, F. Forghani, X. Kong, D. Liu, X. Ye, S. Chen, T. Ding, *Compr. Rev. Food Sci. Food Saf.* **2020**, *19*, 1397.
[54] Y. Huang, C. Yang, X. Xu, W. Xu, S. Liu, *Acta Pharmacol. Sin.* **2020**, *41*, 1141.
[55] A. Sharma, A. Kumar, C. Li, R. K. Sharma, M. T. Swihart, *RSC Adv.* **2020**, *10*, 34254.